Pressure Boundary Treatment in Micromechanical Devices Using The Direct Simulation Monte Carlo Method*

Jong-Shinn WU**, Fred LEE***
and Shwin-Chung WONG***

Two numerical procedures in the Direct Simulation Monte Carlo (DSMC) method, applying particle flux conservation at inflow/outflow pressure boundaries, have been developed to treat the two most important boundary conditions encountered in micromechanical devices involving gaseous flows. The first one is for both specified pressures at inlet and exit; while the second one is for specified mass flow rate and exit pressure. Both numerical procedures have been tested on short and long micro-channels in the slip and transitional regimes. Excellent agreement has been found between the current results and the previous reported numerical results as well as the experimental data for the first type of boundary conditions. Finally, the developed numerical procedures have been applied to backward-facing micro-step gaseous flows to demonstrate its general applicability in more complicated flows.

Key Words: DSMC, Pressure Boundary Treatment, MEMS, Microchannel, Micro-step

1. Introduction

Microelectromechanical systems (MEMS, hereafter) have recently become the focus of a great deal of attention in several research disciplines. These devices are fabricated using processes similar to those in the semi-conductor industry. Potential applications for such devices cover a broad spectrum, including surgical instruments, adaptive optics, data storage, and laminar flow control, etc.[1]-[3]. However, the feature of being of very tiny size brings new challenges in both engineering and fundamental research.

The MEMS devices tend to behave differently than the objects we are used to handling in our daily lives. Because these devices usually appear to be with scales on the order of a micron, the physical processes subject to them can highly differ from those in the macroscopic world[4],[5]. For example, in MEMS devices which often involve gaseous flows through micro-channels, the gas mean free path can be on the order of the characteristic channel dimensions, and thus neglect of rarefaction becomes unacceptable[6]-[8]. The Knudsen number, which is defined as $kn \equiv \lambda/L =$ mean free path/characteristic length and always serves as the index of rarefaction, is no longer negligible in these channels. This fact indicates that treating the gas flows in the micro-channel as a continuum may lead to inaccurate results. Additionally, if the mean free path is large compared to the channel dimensions, it will certainly be much larger than the property gradient scales in the flow, leading to very large local Knudsen numbers. The use of continuum-based techniques in micro-channel analysis and design may therefore lead to inaccurate results. Thus, the conventional computational fluid dynamics (CFD) associated with the Navier-Stokes equations that are based on continuum hypothesis might lead to tremendous deviation on micro-channel flows as mentioned in Nance et al.[9].

For detailed reviews concerning theoretical and

* Received 13th March, 2000
** Department of Mechanical Engineering, National Chiao-Tung University, 1001 Ta-Hsueh Road, Hsin-chu 30050, Taiwan. Corresponding author. E-mail: chongsin@cc.nctu.edu.tw
*** Department of Power Mechanical Engineering, National Tsin-Hua University, Hsinchu 30051, Taiwan

simulation studies on micro-channel gaseous flows, with continuum assumption, they can be found in Beskok et al.[10]-[13] and references cited therein. Although there have been several studies on the micro-channel gas flows on the basis of Navier-Stokes equations[6]-[8],[10]-[13], they are all hampered by the continuum assumption when being applied in transitional regime, i.e. higher Knudsen number flows. One possible solution to resolve this is the direct simulation Monte Carlo (DSMC, hereafter) method[14],[19],[20], developed by Bird. The DSMC method has been used with great success in the prediction of rarefied hypersonic flows, especially in the applications for reentry vehicles into the planetary atmosphere. It is believed that micro gas flows should be well suited for the application of the DSMC[9]. Recently, this has motivated several researchers to apply it to micro-channel gas flows[9],[15]-[17] and are briefly reviewed as follows.

Mavriplis et al.[15] explored the applicability of the DSMC method to the fluid and thermal analysis of two-dimensional channel gas flows. Supersonic, subsonic and pressure driven, low-speed flows were simulated. The results were strongly dependent on Knudsen number and channel aspect ratio.

Ikegawa and Kobayashi[16] developed a DSMC simulator for pressure specified boundary conditions using particle flux conservation concept. However, the conservation concept was applied on the basis of considering the inlet and outlet as a whole, respectively, instead of cell-by-cell basis. This might cause problems when applying to more complicated flows other than channel or pipe flows. Also the out-of-domain particle number flux was computed via the counting of particles flowing out during simulation rather than the approach adopted in current study which will be introduced later.

Piekos and Breuer[17] studied the rarefaction effects in micromechanical devices by DSMC. Their study focused on the slip flow and transitional flow regimes. The unstructured cells and the special treatment of the pressure-specified inflow/outflow (I/O, hereafter) boundary conditions were employed. They kept the specified pressure constant during simulation by adding the particles from outside the flow. Nevertheless, a non-linear pressure distribution along the micro-channel was obtained as well. A trend of increasing pressure curve linearity with increasing rarefaction was also found. This contradicts the experimental findings of Pong et al.[18],[21], but agrees with most other theoretical and numerical studies[8],[11],[13].

Nance et al.[9] investigated the gas flows in long micro-channel via the parallelization of the DSMC code of Bird[14]. For micro-channel gas flows with specified inlet and exit pressures, new procedures of updating I/O boundary conditions were employed. At the inlet, the temperatures and the transverse velocities were given by fixed values, leaving the streamwise velocities to be updated from inside the flow field. At the exit, only the pressure was specified, leaving other properties, such as temperatures and velocities, to be updated from inside the flow field. The theory of characteristics was applied to the exit, assuming inviscid and adiabatic conditions. All updating process was employed for each boundary cell at each time step during the simulation. Besides, the authors suggested a high degree of grid under-resolution in the streamwise direction due to the weaker property gradients, to save the computation time, and were found quite satisfactory for the simulation of micro-channel gas flow, as compared with those of Piekos and Breuer[17].

Summarizing all the previous work on micromechanical devices using the DSMC, there is one important feature identified. That is the flow velocities in these systems are generally less than the speed of sound, which is definitely subsonic and the velocities at the boundaries are not known beforehand. Therefore, the "stream" and "vacuum" boundary conditions typically employed in the DSMC calculations are not physically correct. Instead, one must specially design a numerical procedure to incorporate into the original DSMC algorithm such that the specified inflow and outflow conditions can propagate properly into the flow fields of interest and the velocities and other properties, e.g. temperature, at pressure boundary can be updated as simulation continues.

From the practical points of view in MEMS related flow, there are two types of pressure related boundary conditions which needs to be addressed when applying the DSMC method. The first one is for both specified pressures at inlet and exit; while the second one is for specified mass flow rate and exit pressure. In addition, the potential application of these two types of boundary conditions can often be seen in vacuum technology for computation of pumping speed and maximum compression ratio as well. Therefore, the objectives of the current study is to develop a general numerical procedure for treating pressure related boundary conditions in typical MEMS devices, such as micro-channel and micro-step gaseous flows, using the DSMC method. In summary, this paper is organized as follows in turn. The DSMC method is briefly described, including details of employing particle flux conservation at pressure boundaries. And, then the results and discussion for micro-channel and backward-facing micro-step gas

flows are described in detail. Finally, this paper is concluded by summarizing the important findings of this research.

2. Numerical Method

2.1 Direct simulation Monte Carlo method

The DSMC method[14] had been recognized as the most efficient numerical tool for rarefied gas dynamics. The main features of the DSMC are briefly described in the following.

The basic idea of the DSMC is to calculate practical gas flows through the use of no more than the collision mechanics. The molecules move in the simulated physical domain so that the physical time is a parameter in the simulation and all flows are computed as unsteady flows. An important feature of the DSMC is that the molecular motion and the intermolecular collisions are uncoupled over the time intervals that are much smaller than the mean collision time. Both the collision between molecules and the interaction between molecules and solid boundaries are computed on a probabilistic basis and, hence, this method makes extensive use of random numbers. In most practical applications, the number of simulated molecules is extremely small compared with the number of real molecules. The details of the procedures, the consequences of the computational approximations can be found in Bird[14]. In current study, Variable Hard Sphere (VHS) model and No Time Counter (NTC) is used to simulate the molecular collision kinetics. A structured and uniform Cartesian grid is used to minimize the work required to locate the final position of the moving particles.

In order to perform accurate simulation, general procedures of treating inflow and outflow conditions are developed and incorporated into the basic DSMC algorithm. These procedures are described in detail as follows.

2.2 Inflow/outflow boundary conditions

Two types of I/O boundary conditions are considered in this study. The first type is the one with specified inlet and exit pressures and the second type is with specified mass flow rate and exit pressure. For the simplicity of demonstration, micro-channel gas flow is used as the model problem for the description of two types of I/O boundary conditions. They are described in detail, respectively, in the following.

2.2.1 Boundary conditions with specified inlet and exit pressures (Type I) Consider a two-dimensional flow in a micro-channel with height h and length L. With given inlet pressure P_i, inlet temperature T_i, and exit pressure P_e ($P_e < P_i$), the gas is assumed to flow through the micro-channel. The wall temperatures, T_w, are kept constant. The flow conditions are depicted in Fig. 1.

At the inlet, the treatment is similar to Nance et al.[9]. They are briefly described in the following. The streamwise component, u_i, is determined for each boundary cell m by considering the conservation of particle fluxes across cell m's boundary surface.

For a given mean speed and temperature, the particle flux across a boundary surface with area A in a particular direction can be determined, assuming equilibrium Maxwell-Boltzmann distribution[14], as

$$\frac{\dot{N}}{A}=\frac{nV_{mp}\{\exp(-q^2)+\sqrt{\pi}\,q[1+erf(q)]\}}{2\sqrt{\pi}}, \quad (1.a)$$

where

$$q=\frac{V}{V_{mp}}\cos\theta, \quad (1.b)$$

$$V_{mp}=\sqrt{\frac{2kT}{m}}. \quad (1.c)$$

Considering the interface of boundary cell m, we can apply Eq. (1) to determine the rate of particles crossing in either direction. Applying the particle flux conservation at the boundary gives

$$(u_i)_m=\frac{(\dot{N}_+-\dot{N}_-)_m}{n_i(A)_m}, \quad (2)$$

where $(\dot{N}_+)_m$ and $(\dot{N}_-)_m$ are computed using the latest updated $(u_i)_m$ and sampled $(u_1)_m$ in the boundary cell m, respectively, from Eq. (1). The value $(u_i)_m$ and $(u_1)_m$ will be varied during the simulation and eventually attain a nearly constant value as the steady state is reached.

At the exit, on the other hand, all fluid properties except pressure are computed from the simulation. Again, we apply the concept of particle flux conservation for the exit, rather than applying the theory of characteristics[9]. Then, the similar procedure for inlet conditions is carried out for updating $(u_e)_m$. Note that the exit temperature, $(T_e)_m$, which is not given in advance, is enforced to be equal to the temperature of each exit boundary cell m, i.e.,

$$(T_e)_m=(T_2)_m, \quad (3)$$

where $(T_2)_m$ is initially guessed and then evolves during the simulation. Additionally, the exit number density is computed using the equation of state as

$$(n_e)=\frac{P_e}{k(T_2)_m}. \quad (4)$$

Combining Eqs. (3), (4) and applying the enforcement of conservation of particle flux, Eq. (2), at the outflow pressure boundary, the simulated exit pressure is found to be consistent with the specified exit pressure and the mass conservation holds as well automatically.

The main difference between the current study and Nance et al.[9] is that we have applied particle flux conservation at both the pressure boundaries, inlet and exit in this case, while Nance et al. used it only at

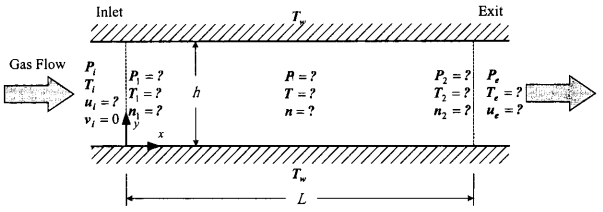

Fig. 1 The sketch of micro-channel gas flow with Type I boundary conditions

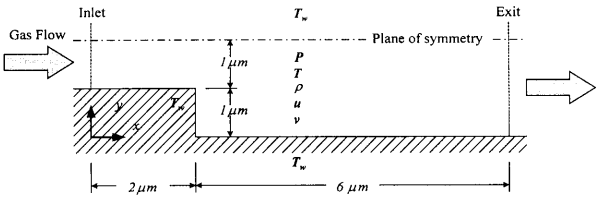

Fig. 2 The sketch of backward-facing micro-step gas flow

the inlet and apply theory of characteristics for subsonic flows at the exit, assuming adiabatic and isentropic flow conditions. Current approach ensures the continuity of flows (mass conservation) automatically when the flow reaches steady state. Hence, we expect the current approach would be superior to that of Nance et al.[9] in terms of its generality in application, since the only assumption is in thermal equilibrium at the pressure boundary. We have also found that the number of samples required for steady state solution using current approach are fewer than those of Ref.(9), which can be seen clearly later.

2.2.2 Boundary conditions with specified mass flow rate and exit pressure (Type II) Consider the same micro-channel with constant mass flow rate $\dot{M}$ through this channel, with upstream temperature at T_i and downstream pressure at P_e. Both walls maintain their temperatures at T_w, respectively. The sketch of this flow is similar to Type I as in Fig. 1 except those mentioned in the above.

At the inlet, the streamwise velocity component is decided by $\dot{M}$. The integral $\dot{M}=\int_0^h \rho(x, y)u(x, y)dy$ is replaced with finite summation of the average value in each boundary cell with,

$$\begin{aligned}\dot{M} &= \sum_1^{NCY}(\rho_i)_m(u_i)_m\Delta y \\ &= m\sum_{m=1}^{NCY}(n_i)_m(u_i)_m\Delta y \\ &= mh\sum_{m=1}^{NCY}(n_i)_m(u_i)_m\frac{\Delta y}{h}.\end{aligned} \tag{5}$$

In the above, "NCY" denotes the number of cells in the transverse direction, and Δy represents the cell height. Notice that $\dot{M}/mh$ is actually the net particle flux crossing some particular cross-section in this unit-depth channel. We rewrite Eq.(5) as the following,

$$\left(\frac{\dot{N}}{A}\right)_{net}\equiv\frac{\dot{M}}{mh}=\sum_1^{NCY}(n_i)_m(u_i)_m\frac{\Delta y}{h}. \tag{6}$$

Because there is no way to determine $(u_i)_m$ for each m by examining Eq.(6), an alternative hypothesis of uniform velocity is applied to the inlet conditions:

$$u_i\equiv(u_i)_1=(u_i)_2=\cdots=(u_i)_{NCY}. \tag{7}$$

By defining the average inlet number density as

$$\bar{n}_i=\sum_1^{NCY}(n_i)_m\frac{\Delta y}{h}, \tag{8}$$

Combination of Eqs.(6) and (7) results in the following expression for inlet streamwise velocity associated with constant mass flow rate,

$$u_i=\frac{1}{\bar{n}_i}\left(\frac{\dot{N}}{A}\right)_{net}=\frac{\dot{M}}{\bar{n}_i mh}. \tag{9}$$

in Eqs.(8) and (9), $\dot{M}$, m, h and Δy are all constants, while $\bar{n}_i$ is determined by $(n_i)_m$. It is reasonable to approximate $(n_i)_m$ as the number density interior to the inlet boundary cell m, i.e.,

$$(n_i)_m=(n_1)_m, \tag{10}$$

which might differ from cell to cell and vary from one time-step to the next. Thus, during the computation, $\bar{n}_i$ and in turn u_i will be updated in each time-step.

At the exit, similar treatment to Type I pressure boundary is employed. We again use Eq.(1) to compute the particle flux across the outflow boundaries. The positive particle flux $\left(\frac{\dot{N}_+}{A}\right)_m$ is calculated based on $(u_2)_m$, $(n_2)_m$ and $(T_2)_m$, and thus is employed to introduce particles at the exit boundary. Similarly, the negative particle flux $\left(\frac{\dot{N}_-}{A}\right)_m$ can also be calculated with Eq.(1), based on, $(u_e)_m$, $(n_e)_m$ and $(T_e)_m$, which are updated during the computation. After the positive and negative particle fluxes are computed, the streamwise velocities at each boundary cell of the outflow boundaries are enforced via Eq.(2) at each time step during simulation.

3. Results and Discussion

The algorithms described above are used to simulate the gas flows in short and micro-channels (Fig. 1) and short backward-facing micro-step (Fig. 2). Argon is specified as the working gas for all the cases considered except in the case of long micro-channel. Knudsen number based on the channel height and exit pressure condition ranges from slip flow ($Kn=0.05$) to transitional flow ($Kn=10$) regimes. Similar to Nance et al.[9], grid relaxation strategy in the streamwise direction is applied to reduce the computational load for long micro-channel computation. The results in the following are organized as

follows: Micro-channel gas flows are first used to verify current treatment of pressure related boundary conditions and compared with previous reported work. Then, the numerical procedure is applied to backward-facing micro-step to demonstrate its general applicability to more complicated gas flows.

3.1 Micro-channel flows

In this sub-section, verification of the developed treatment of two types of I/O boundary conditions is described first, followed by the general flow properties, then the Knudsen number and pressure ratio effects on mass flow rate, and finally the Knudsen number effects on flow properties distribution are detailed in turn.

3.2 Verification of inflow/outflow boundary treatment

A short micro-channel flow was used as the test case for the verification of I/O treatment. The selected short channel has dimensions of 5 μm in length and 1 μm in height, with aspect ratio of 5. The upstream temperature T_i is 300 K. The temperature of both walls, T_w, is 300 K, assuming full thermal accommodation. Constant inlet to exit pressure ratio $P_i/P_e=3$ is specified with exit Knudsen number equal to 0.05. The results of centerline streamwise velocity, pressure and temperature along with those of Ref. (9), are illustrated in Fig. 3 for comparison. It is found that the agreement between Type I and Nance et al.'s is excellent. Also both procedures are able to exactly predict the specified inlet and exit pressures, which are often over predicted otherwise using conventional treatment in the DSMC as shown in Refs. (9) and (18). Similar tests have been conducted for the same configuration with different Knudsen number. The present results agree very well with those of Ref.(9). This clearly demonstrates that proposed procedure is correct and robust.

For the Type II boundary conditions, we used the mass flow rate (4.5×10^{-4} kg/sec), obtained from the Type I boundary conditions and the same exit pressure. Thus, we can verify if the current treatment of Type II boundary conditions is successful or not, by comparing the simulated pressure ratio (inlet to exit) with the expected value of 3.0. Simulated results are also presented in Fig. 3. As can be seen all the predicted flow properties are almost the same as those of Type I boundary conditions, except the streamwise velocity and temperature near the inlet. This is mainly due to the enforcement of uniform velocities at the inlet for the Type II boundary conditions as described in previous section. Nevertheless, the proposed treatment of Type II boundary conditions successfully predicts most of the flow properties.

We have also tried to understand how fast the flow field "converges" to the steady state solution by monitoring the mass flow rates both at the inlet and exit, respectively. Typical results are shown in Fig. 4 for long micro-channel case (Ar, $Kn_e=0.1$, $P_i/P_e=3$, $L/h=30$). We can see that boundary conditions proposed by Nance et al.[9] cause more violent fluctuations of inlet and exit mass flow rate than the present boundary condition (Type I) during flow development. In addition, the instantaneous mass flow rate curves at the inlet and the exit for present boundary conditions (Fig. 4(b)) appear to merge much faster. This can be seen more clearly if we plot the data in terms of relative mass flow rate (ratio of instantaneous mass flow rate to final steady value) as a function of time. This should be attributed to the particle flux conservation enforced both at the inlet and exit in the current approach, rather than that only applied at the inlet in Ref.(9). This implies that the present treatment of pressure boundary conditions (Type I) requires fewer samplings of particles to reach the steady state solution. Similar trends have been found for shorter channel and other flow conditions as well.

3.3 General flow properties

The typical gas flow properties obtained using Type I boundary conditions are shown as three-dimensional (3-D) surfaces in Fig. 5. The test configuration is listed as follows: Ar, $Kn_e=0.1$, $P_i/P_e=3$, $L/h=5$. Note that typical cell size ratio to the local mean free path is about 0.5 and the number of particles per cell is in the range of 10 - 20.

In Fig. 5(a), we can see that streamwise velocity is accelerated along the channel, with a nearly parabolic profile in the transverse direction. The compressibility effect is very strong due to the large pressure gradient (short channel), leading to an increasing gradient of streamwise velocity. The streamwise velocity acceleration is larger near the exit due to the larger pressure gradient near the exit. Velocity slips at both walls are significant and increase in the downstream direction because of the rarefaction effect.

The pressure, in Fig. 5(b), decreases nonlinearly along the channel. This nonlinearity results from the compressibility in the gas flows. The isobars appear to be straight lines in the transverse direction, which justifies the assumption of $\frac{dP}{dy}=0$ in most theoretical studies[6]-[8],[11],[13].

The variation in density distribution, in Fig. 5(c), is similar to that of the pressure, although the density decrease is less pronounced. At a fixed x, the maximum density appears near the centerline ($y=0.5$ μm), where the maximum flow speed is attained.

The gas temperature in a short channel, in Fig. 5(d), decreases remarkably, especially near the exit.

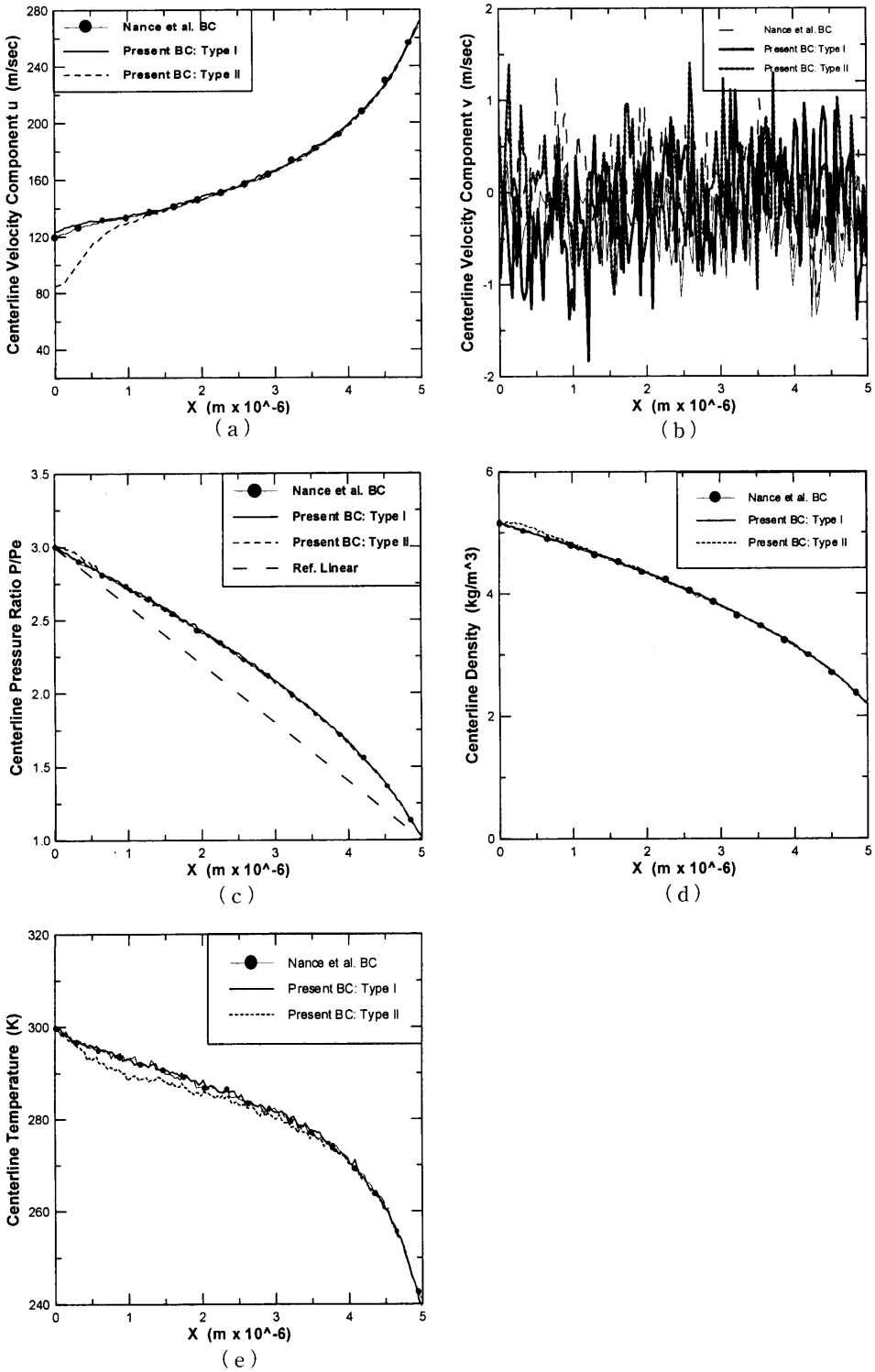

Fig. 3 Comparison of centerline low properties with different I/O treatment (Ar, Kn_e=0.05, L/h=5, all dimensions in micrometer)

This temperature drop due to gas expansion (decreasing pressure) is enhanced by the strong pressure gradient $\frac{dP}{dx}$ near the exit. With $P=\rho RT$, the rapid temperature drop is responsible for the less pronounced density drop. In addition, the temperature slips at both walls are apparent and increase in the downstream direction due to rarefaction as well.

3.4 Knudsen number and pressure ratio effects on mass flow rate

Applying Type I boundary conditions, we use Helium as the working gas and the same configuration

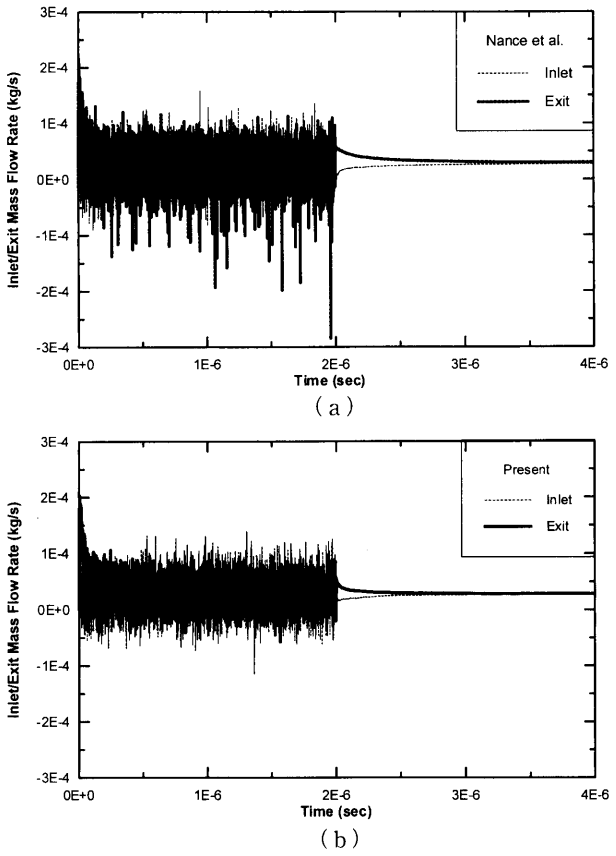

Fig. 4 Typical time history of inlet and exit mass flow rate with different I/O treatment. (Ar, Kn_e=0.05, P_i/P_e=3, L/h=30)

except for a longer channel with aspect ratio of 30. The results, along with theoretical prediction by Beskok et al.[11], are presented in Fig. 6, which provides the information about how the mass flow rate depends on the pressure ratio and Knudsen number. Although the experimental data of Arkilic et al.[7] (represented by circles on the plot, Kn_e=0.165) are

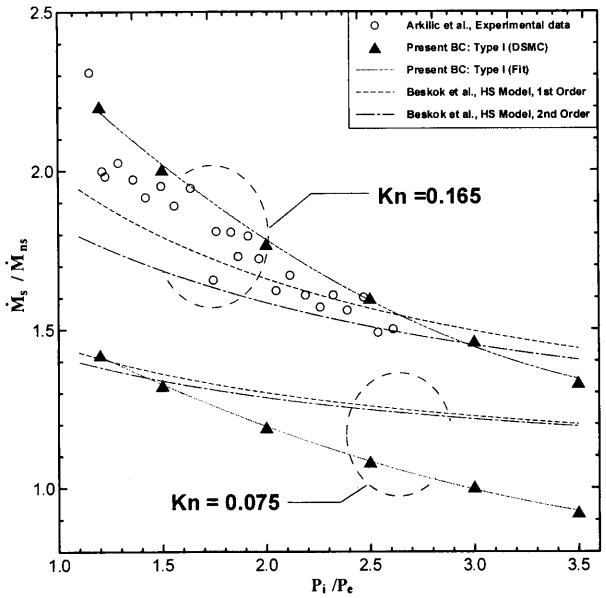

Fig. 6 Variation of normalized mass flow rate as a function of pressure ratio. (He, L/h=30)

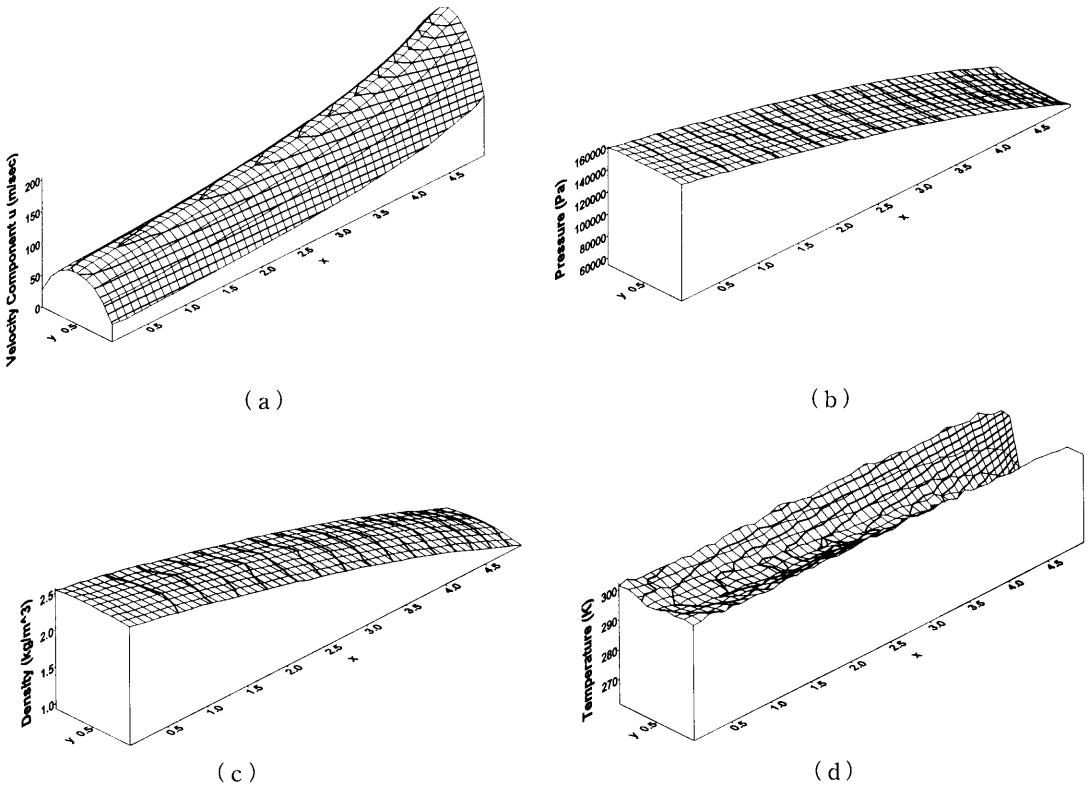

Fig. 5 Typical 3-D surface plot of flow properties in the short micro-channel. (Ar, Kn_e=0.05, L/h=5, all dimensions in micrometer)

highly scattered due to the experimental difficulties involved in measuring the very small mass flow rates in micro-channels, the trend of decreasing $\dot{M}_s/\dot{M}_{ns}$ with increasing P_i/P_e is obvious. Note that $\dot{M}_{ns}$ is the no-slip mass flow rate obtained from continuum analysis[11]. At low pressure ratios, the DSMC predicted or measured mass flow rates are even 100% higher than those predicted by the continuum theory. The theoretical model seems to predict the data quite well for $1.7 < P_i/P_e < 2.6$, which we believe to happen by chance at such high Kn ($=0.165$). For the whole range of P_i/P_e considered, the DSMC results seem to yield higher $\dot{M}_s/\dot{M}_{ns}$ than the experimental data. But they are still within the experimental uncertainties considering how difficult it is to measure such tiny mass flow rate on the order of 10^{-13} kg/s as mentioned in Arkilic[7]. However, it should be noted that the DSMC method is the only one that predicts the same trend of $\dot{M}_s/\dot{M}_{ns}$ as the experimental data throughout the whole range of P_i/P_e considered. For the results with $Kn_e=0.075$, only prediction by DSMC method is plotted along with corresponding theoretical data, since no experimental data are available in the literature. All the theoretical data deviate from the DSMC results severely as P_i/P_e is over 1.5. This is because the isothermal assumption is inadequate for strongly compressible flows at such a low Knudsen number, $Kn_e=0.075$, as explained earlier.

We can conclude that, as far as the prediction of the mass flow rate is concerned, the theoretical models should work for low Knudsen number flows at low pressure ratio, while for flows of high pressure ratio at high Knudsen number (in slip and transitional flows), only the DSMC method is adequate.

3.5 Knudsen number effects on flow properties distribution

The effects of compressibility and rarefaction on the longitudinal flow properties are illustrated in Fig. 7 for micro-channels with pressure ratio of 3 and aspect ratio of $L/h=5$ and 30. The pressure, streamwise velocity and temperature will be discussed in turn in the following.

All DSMC predictions indicate that the longitudinal pressure decreases nonlinearly with streamwise location as stated previously. Stronger rarefaction (higher Kn) tends to result in a more linear pressure distribution. This obviously contradicts the results of Pong et al.[21]. On the other hand, at fixed P_i/P_e and Kn_e, stronger compressibility exists in a shorter channel due to the higher pressure gradient. Comparing the cases with two different aspect ratios in Figs. 7 (a) and 7(b) indicates that higher compressibility (shorter channel) results in stronger nonlinearity of the pressure distribution. For $Kn_e \geq 1$, the flow becomes collisionless and flow properties becomes indistinguishable. The resulting pressure becomes almost linear with streamwise location, which is a well-known result from free-molecular analysis[22].

For $Kn_e \geq 1$, the DSMC solution seems to over predict the pressure ($\sim$2%) near the inlet or exit, especially for short channels (Fig. 7(a)). This might result from the equilibrium Maxwellian distribution, which has been used in Eq.(1.a) for introducing particles into the flow domain. For higher rarefaction (higher Kn) and pressure gradient (shorter channel), the local Knudsen number ($Kn_x=\lambda/[T/(\partial T/\partial x)]$ or $\lambda/[u/(\partial u/\partial x)]$) becomes so large that the equilibrium Maxwellian distribution no longer holds. This might require special treatment by using the Chapmann-Enskog distribution function in the problem and deserves future study to resolve this non-equilibrium condition at the pressure boundaries.

The streamwise velocity curves with $P_i/P_e=3$ and various Kn_e are plotted in Figs. 7(c) and 7(d) for $L/h=5$ and 30, respectively. In Figs. 7(c) and 7(d), the centerline streamwise velocities increases with streamwise location with larger positive gradient near the exit due to the larger pressure gradient observed at the same location (Fig. 7(a)). For the short channel case, the acceleration due to the pressure gradient (or compressibility) is remarkable or $Kn_e=0.05$ and 0.1 (Figs. 7(c)) but less pronounced for higher Kn_e (Fig. 7(d)). It indicates that the rarefaction effect suppresses flow acceleration due to compressibility. However, for $Kn_e \geq 1$, the centerline $\boldsymbol{u}$ curves seem to be "invariant". This is because, as $Kn_e \geq 1$, the flow is highly rarefied and tends to be in the free-molecular regime so that the molecular collision frequency becomes very low. Therefore, the collision mechanism employed by the DSMC method does not make much change to the flow field properties. Similar results are also obtained for the long channel (Fig. 7(d)). In Fig. 7(d), the pressure gradient is merely about 1/6 of the corresponding case in Fig. 7(c), leading to a weaker compressibility effect and hence weaker flow acceleration. This explains why each streamwise velocity in Fig. 7(c) is lower than its corresponding one in Fig. 7(d).

The temperature profiles at different Kn_e are depicted in Fig. 7(e) and 7(f), for the $L/h=5$ and 30, respectively. In the figures, the constant temperature profile $T=300$ K is plotted as well for comparison. For the short channel ($L/h=5$), the gas temperature drops rapidly, for the reason given in the above. From Fig. 7(e), it is found that the more rarefied the gas flow is, the less the temperature drop will be, due to the less relative compressibility involved. However, for $Kn_e \geq 1$ (Fig. 7(e)), the temperature profiles are

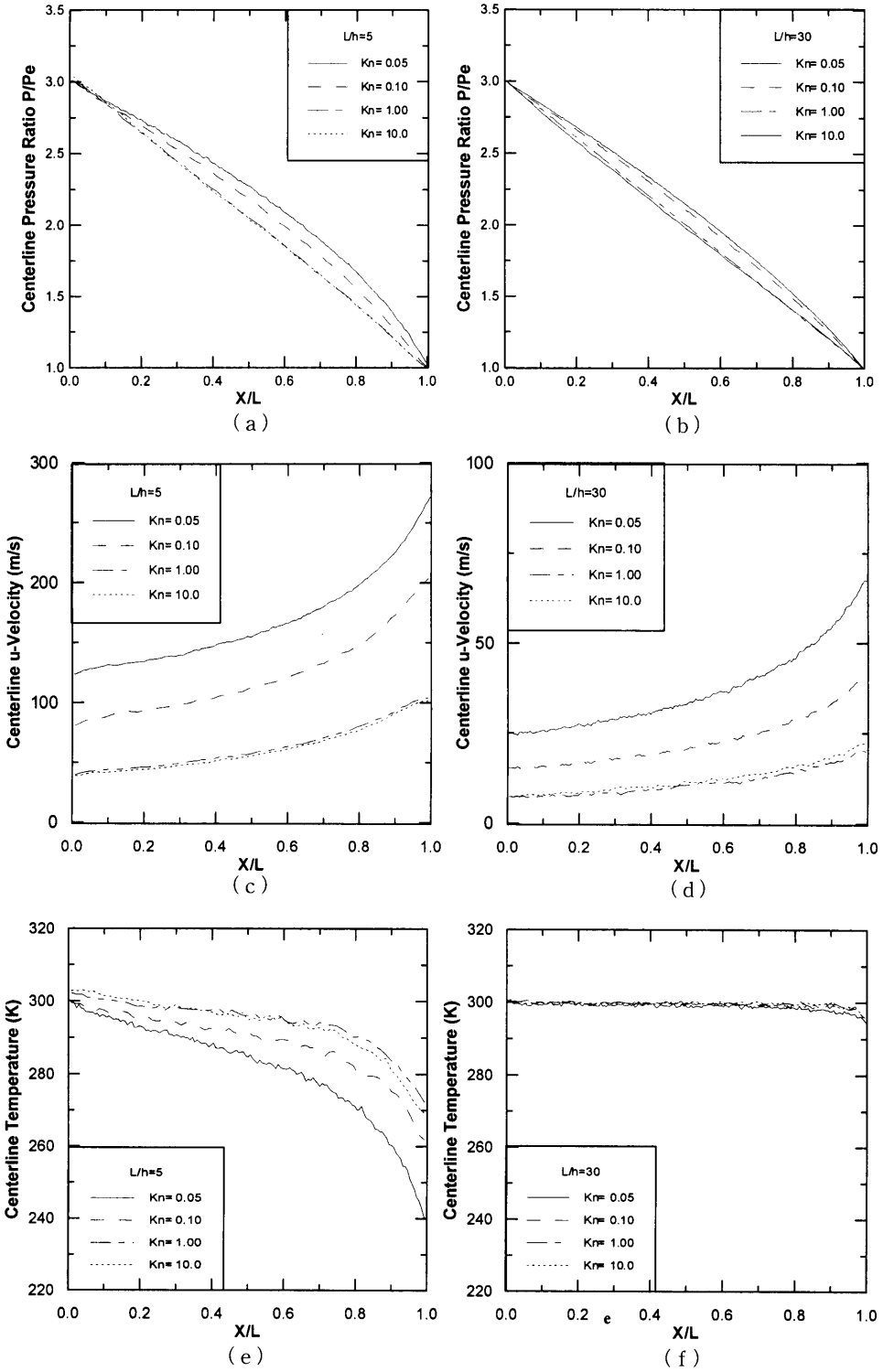

Fig. 7 Normalized flow properies as a function of Kn and x/L. (Ar, $P_i/P_e=3$, $L/h=5, 30$)

almost invariant with Kn_e similar to the streamwise velocity. This could again result from the low collision frequency in highly rarefied flows. Another finding for the highly rarefied flows with $Kn_e \geq 1$ is the increasing deviation of the simulated and specified inlet temperatures with increasing Kn_e. This is due to the same non-equilibrium phenomena caused by high local Knudsen number, as mentioned in the above.

For the long micro-channel case (Fig. 7(f), $L/h=30$), in which the pressure gradient is smaller, the gas temperature profiles appear to be nearly constant, except near the exit, in contrast to those in the short channel ($L/h=5$). The obvious temperature drop near the exit is because of the larger pressure gradient near

the exit. Since the non-equilibrium effect is not pronounced due to smaller property gradients, there is no apparent temperature deviation found at the inlet and exit. The fact that the temperature profiles appear to be invariant with Kn_e indicates a weaker effect of rarefaction than compressibility on temperature. Thus, the isothermal condition often assumed in most theoretical modeling should be adequate for long micro-channel analysis.

3.6 Backward-facing micro-step flows

So far we have developed two I/O treatments, with emphasis on the particle flux conservation at the pressure boundaries, and both are verified to be successful in simulating gas flows in micro-channels, which possess uniform cross sections and almost zero pressure gradient in transverse the direction in the flow field. We thus wonder if the developed I/O treatment can be applied to more complicated micro-scale gas flows, such as micro-step (e.g., backward-facing) flows. The reason we have chosen backward-facing micro-step flow is due to its simple geometry but varying area along the channel and non-negligible pressure gradient in the transverse direction in the flows. Hence, we applied the present I/O treatment (both Types I and II) to simulate the backward-facing micro-step gas flows. Since the purpose is to demonstrate the general applicability of the treatment of pressure boundary, only the general physical features of the results are discussed here.

The geometry and dimensions of the 2-D micro backward-facing step are depicted in Fig. 2. To save computational time, only one half of the flow field is considered by taking the advantage of the symmetric plane.

The effect of the rarefaction is investigated by varying the exit Knudsen number, Kn_e. Argon is again used in the simulation. The temperatures of the inflow gas and all walls are fixed at 300 K.

3.7 General flow properties

Typical results (3D surface) of simulated backward-facing micro-step gas flows by Type I I/O treatment are depicted in Fig. 8 for $Kn_e=0.1$, with $P_i/P_e=3$. The related flow properties are discussed in the following.

From Figs. 8(a) and 8(b), in the entrance duct, the streamwise velocity is accelerated with a nearly parabolic profile in the transverse direction due to the strong pressure drop. The maximum u-velocity occurs at about $x=3$ μm, which is located in the early portion of expanded duct. Afterwards, u-velocity decelerates and then accelerates slightly to the exit. The deceleration of u-velocity mainly results from the enlargement of the cross-section, which leads to stronger molecular motion in the transverse direction, especially in the downward direction to the region behind the step. However, the later acceleration of u-velocity is mainly caused by the pressure gradient imposed. At the same time, the velocity slip increases dramatically along in the expanded duct due to the high rarefaction behind the step. At this $Kn_e=0.1$, a negative streamwise velocity and positive transverse velocity is found right behind the step, indicating a circulation exists there. As Kn_e becomes larger ($Kn_e=1.0$), which is shown in Fig. 9(b), the streamwise velocity behind the step becomes more positive and eventually this circulation disappears. This is due to the fewer molecular collisions occurring in more rarefied flows such that the molecules coming from the narrow duct have much less chance of bouncing back to the region behind the step, which is the main mechanism of circulation occurring behind the step. In summary, the circulation behind the step tends to be more obvious as Kn decreases, as can be clearly seen from the streamlines presented in Fig. 9.

From Fig. 8(c), the simulated pressure decreases nonlinearly in the narrow entrance duct. In the expanded portion after the step ($\boldsymbol{x}>2$ μm), the pressure drop is rather slight. At this moderate rarefaction with $Kn_e=0.1$, the centerline ($\boldsymbol{y}=2$ μm) pressure first increases slightly and then decreases slightly for $\boldsymbol{x}>2$ μm, while at higher rarefaction, it decreases monotonically (not shown here). On the other hand, the pressure behind the step even becomes negative (compared to the exit pressure), while it is becomes positive for higher Kn flows. For all Kn_e, a local minimum pressure is found behind the step (2 μm$\leq \boldsymbol{x}<3$ μm, $\boldsymbol{y}<3$ μm). However, the increase of Kn_e tends to elevate the ratio of this local minimum pressure to the inlet pressure. For highly rarefied flows ($Kn_e\geq 1$), the pressure distribution appears to be insensitive to Kn_e because the molecular collision mechanism is no longer dominant. Most importantly, the specified pressures at the inlet and exit are nearly predicted as the steady state is reached. As in the micro-channel gas flows, the density surfaces (Fig. 8(d)) are similar to those of the pressure (Fig. 8(c)). Also, the variation in density is smaller compared with the pressure.

Temperature drop is observed near the end of the narrow entrance region (Fig. 8(e)). However, this temperature drop, caused by sudden area expansion, is diminished with higher rarefaction, which tends to make the temperatures more uniform in the flow field.

4. Conclusions

The present study has successfully developed two important numerical treatments of pressure related boundary conditions in the DSMC method by applying particle flux conservation. The new treatment I/O

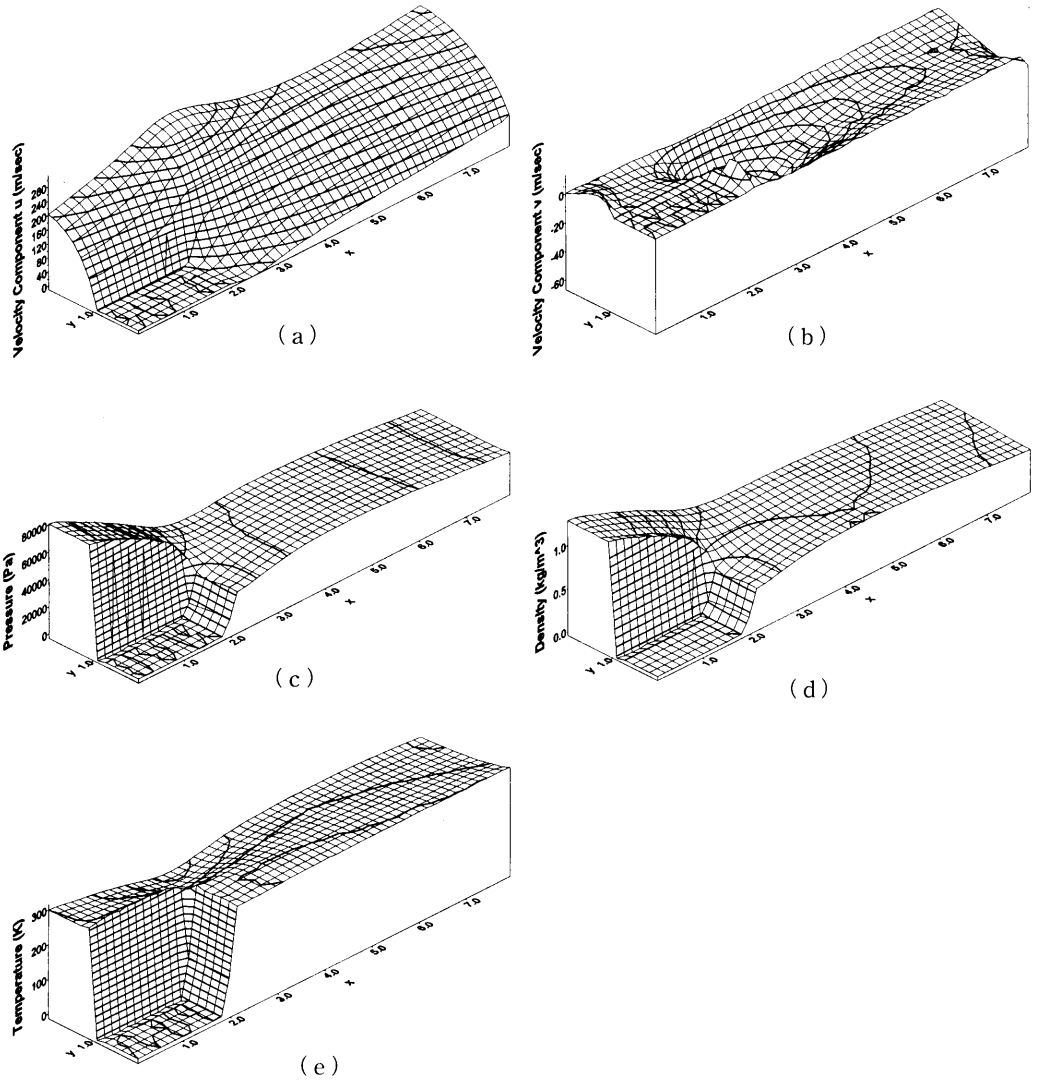

Fig. 8 Typical 3-D surface plot of flow properties in the backward-facing micro-step gas flow with Type I boundary conditions (Kn_e=0.1)

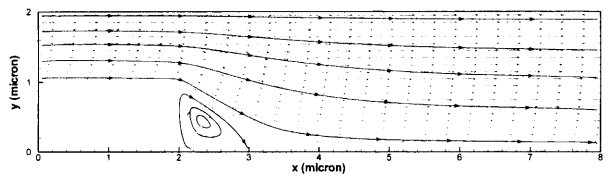

(a) Kn_e=0.1

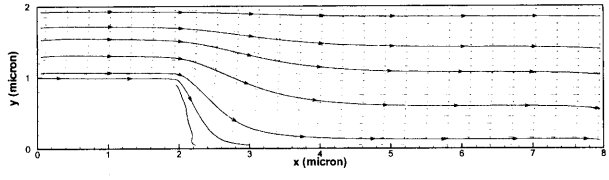

(b) Kn_e=1

Fig. 9 Velocity vectors and streamlines in the backward-facing micro-step gas flow (Ar; Kn_e=0.1, 1.0)

treatment has been applied to micro-channel and backward-facing micro-step gas flows to establish its general applicability. In summary, the general conclusions can be listed as follows.

(1) Current treatment of pressure specified I/O has been proved to be superior to that developed by Nance et al.[9] in terms of the amount of sampling required for steady-state solution. This is mainly due to the particle flux conservation concept applied at both the pressure boundaries such that the conservation of mass is automatically ensured.

(2) The applications of the current I/O treatment to micro-channel gas flows have demonstrated that the streamwise velocity is accelerated along the channel and pressure decreases nonlinearly with streamwise location, while increasing Kn will eventually make the flow properties invariant and pressure distributed linearly along the channel due to rarefaction.

(3) General applicability of the current treatment of pressure boundary has been established by the application to backward-facing micro-step gas flows. Results have shown that increasing rarefaction tends to destroy the circulation behind the micro-step, often observed in continuum analysis. Further study on the detailed physics of micro-step gasflows is worthwhile.

Due to the rapid development of MEMS, test of the current treatment of pressure related boundary conditions to micro-scale gas flows with more complex geometry is highly desired and currently in progress.

References

(1) Alexander, F.J., Garcia, A.L. and Alder, B.J., Direct Simulation Monte Carlo for Thin-Film Bearings, The Physics of Fluids, Vol. 6, No. 12 (1994), pp. 3854-3860.

(2) Richter, M., Woias, P. and Weiß, D., Micro-channels for Applications in Liquid Dosing and Flow-Rate Measurement, Sensors and Actuators, A 62 (1997), pp. 480-483.

(3) Shoji, S. and Esashi, M., Microflow Devices and Systems, Journal of Micromechanical and Microengineering, Vol. 4, No. 4 (1994), pp. 157-171.

(4) Baker, J., Calvert, M.E., Power, D.J. and Chen, E.T., On the Role of the Knudsen Number with Respect to Heat Transfer in Micro-Scale Flows, IEEE 31st Proceedings of the Intersociety Energy Conversion Engineering Conference, Piscataway, NJ, USA, (1996), pp. 1396-1401.

(5) Ho, C.M. and Tai, Y.C., Micro-Electro-Mechanical-Systems (MEMS) and Fluid Flows, Annual Review of Fluid Mechanics, (1998), pp. 1-34.

(6) Arkilic, E.B., Breuer, K.S. and Schmidt, M.A., Gaseous Flow in Micro-channels, Application of Microfabrication to Fluid Mechanics, ASME, FED-Vol. 197 (1994), pp. 57-66.

(7) Arkilic, E.B., Measurement of the Mass Flow and Tangential Momentum Accommodation Coefficient in Silicon Micromachined Channels, Ph. D. Thesis, FDRL TR 97-1, MIT, Jan. (1997).

(8) Arkilic, E.B., Schmidt, M.A. and Breuer, K.S., Gaseous Slip Flow in Long Micro-channels, Journal of Microelectromechanical Systems, Vol. 8, (1997), pp. 167-178.

(9) Nance, R.P., Hash, D.B. and Hassan, H.A., Role of Boundary Conditions in Monte Carlo Simulation of Microelectromechanical Systems, Journal of Thermophysics and Heat Transfer, Technical Notes, Vol. 12, No. 3 (1998), pp. 447-449.

(10) Beskok, A. and Karniadakis, G.E., Modeling Separation in Rarefied Gas Flows, 28th AIAA Fluid Dynamics Conference and 4th AIAA Shear Flow Control Conference, Snowmass Village, CO, (1997).

(11) Beskok, A. and Karniadakis, G.E., Simulation of Heat and Momentum Transfer in Complex Microgeometries, AIAA Journal of Thermophysics and Heat Transfer, Vol. 8, No. 4 (1994), pp. 647-655.

(12) Beskok, A., Karniadakis, G.E. and Trimmer, W., Rarefaction, Compressibility and Thermal Creep Effects in Micro-Flows, Journal of Fluids Engineering, Vol. 118 (1996), pp. 448-456.

(13) Harley, J.C., Huang, Y., Bau, H.H. and Zemel, J. N., Gas Flow in Micro-channels, Journal of Fluid Mechanics, Vol. 284 (1995), pp. 257-274.

(14) Bird, G.A., Molecular Gas Dynamics and the Direct Simulation of Gas Flows, Oxford Engineering Science, (1994), Oxford University Press, New York, NY.

(15) Mavriplis, C., Ahn, J.C. and Goulard, R., Heat Transfer and Flowfields in Short Micro-channels Using Direct Simulation Monte Carlo, Journal of Thermophysics and Heat Transfer, Vol. 11, No. 4 (1997), pp. 489-496.

(16) Ikegawa, M. and Kobayashi, J., Development of a Rare+1X Rarefied Flow Simulator Using the Direct-Simulation Monte Carlo Method, JSME Int. J., Ser. 2, Vol. 33, No. 3 (1990), pp. 463-467.

(17) Piekos, E.S. and Breuer, K.S., Numerical Modeling of Micromechanical Devices Using the Direct Simulation Monte Carlo Method, Transactions of the ASME Journal of the Fluids Engineering, Vol. 118 (1996), pp. 464-469.

(18) Liu, J., Tai, Y.C. and Ho, C.M., MEMS for Pressure Distribution Studies of Gaseous Flows in Micro-channels, IEEE Proceedings of MEMS, (1995), pp. 209-215.

(19) Muntz, E.P., Rarefied Gas Dynamics, Annual Review of Fluid Mechanics, Vol. 21 (1989), pp. 387-417.

(20) Oran, E.S., Oh, C.K. and Cybyk, B.Z., Direct Simulation Monte Carlo: Recent Advances and Applications, Annual Review of Fluid Mechanics, Vol. 30 (1998), pp. 403-441.

(21) Pong, K.C., Ho, C.M., Liu, J. and Tai, Y.C., Nonlinear Pressure Distribution in Uniform Micro-channels, ASME Application of Microfabrication to Fluid Mechanics, FED-Vol. 197 (1994), pp. 51-56.

(22) Gombosi, T.I., Gaskinetic Theory, (1994), Cambridge University Press.